Free-Energy Barrier at Droplet Condensation

Andreas Nußbaumer, Elmar Bittner and Wolfhard Janke

Institut für Theoretische Physik and Centre for Theoretical Sciences (NTZ), Universität Leipzig, Postfach 100 920, D-04009 Leipzig, Germany

We discuss several aspects of a Monte Carlo computer simulation study of the condensation of macroscopic droplets emerging in the two-dimensional Ising lattice-gas model. By varying the particle density at fixed temperature we monitor the droplet formation in detail and compare our results with recent analytical predictions in the infinite-volume limit. Three different lattice discretizations are considered which are found to yield very similar results when presented in properly scaled variables. Particular emphasis is placed on the free-energy barrier associated with droplet formation and its implication for multimagnetical simulations.

§1. Introduction

The precise mechanism for the formation of a first large droplet in condensing systems is one of the fundamental problems in statistical physics. Early studies date back to the seminal analytical work by Fisher[1)] and computer simulations by Binder, Kalos and Furukawa.[2),3)] Over the years this problem has been taken up and further advanced in several numerical studies.[4)] Particularly noteworthy is the careful analysis of Hager and Neuhaus,[5)] which stimulated new theoretical[6)–8)] and numerical[9)–12)] work. Here, we follow the mathematical considerations of Biskup et al.,[6),7)] which are based on an equilibrium framework and result in largely model independent scaling predictions for the condensation process in the infinite-volume limit.

One purpose of the present study is to investigate by how much these asymptotic predictions are affected by finite-size effects. The second goal is to test the degree of universality suggested by the analytical treatment. Finally, we also present new results on the free-energy barrier associated with the droplet formation. After briefly recalling the Ising model and its lattice-gas interpretation in §2, the theoretical scaling predictions are summarized in §3. In §4 the results of our quite extensive Monte Carlo computer simulations are discussed, and in §5 we close with a summary and a brief outlook to future work.

§2. Model

Throughout this paper we consider the Ising model with Hamiltonian

$$\mathcal{H} = -J \sum_{\langle i,j \rangle} \sigma_i \sigma_j \,, \quad \sigma_i = \pm 1 \,, \quad J = 1 \,, \tag{2·1}$$

where $\langle i,j \rangle$ denotes short-range interactions and the spins σ_i, $i = 1, \ldots, V$, live on the sites of a regular lattice with periodic boundary conditions to be specified below. Denoting in an arbitrary spin configuration the number of spins pointing up (down)

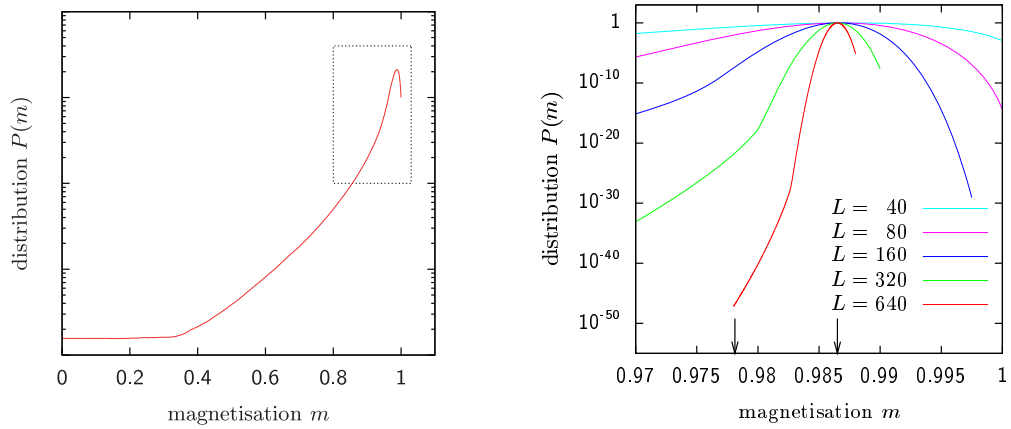

Fig. 1. Left: Sketch of the probability distribution $P(m)$ of the magnetisation in an Ising model below the Curie temperature T_c. The marked box indicates the region where the evaporation/condensation transition takes place. Right: Variation of $P(m)$ for next-neighbour interactions on a square lattice in the peak region with increasing system size L. For the larger systems a cusp develops for $m < m_0$, which signals the transition from the evaporated phase (low density) on its right towards the maximum to the condensed phase (high density) on its left side. The two arrows on the x-axis indicate for $L = 640$ the range of data points used later in Fig. 5.

by n_+ (n_-), one obviously has $V = n_+ + n_-$ and the magnetisation can be written as

$$M = Vm = \sum_i \sigma_i = n_+ - n_- = V - 2n_- = 2n_+ - V\,, \tag{2·2}$$

such that $\rho_- \equiv n_-/V = (1-m)/2$ and $\rho_+ \equiv n_+/V = (1+m)/2$ are the corresponding densities. By interpreting down spins as particles and up spins as vacancies (or, due to symmetry, vice versa), one arrives at a lattice gas interpretation with the magnetisation m controlling the particle density.

Below the Curie temperature T_c, the magnetisation distribution $P(m)$ of large but finite systems exhibits in zero magnetic field the typical double-peak structure depicted in the left plot of Fig. 1, with the peak maximum located close to the infinite-volume magnetisation m_0. Due to the Z_2 symmetry of the model only the right peak is shown. The blow-up of the marked box in the right plot of Fig. 1 features for the larger systems a cusp at a system size dependent magnetisation $m_c < m_0$. This is the signal for the evaporation/condensation point where the particles in the lattice-gas picture tend to condense into a single large droplet. The Gaussian shape of the peak to the right of the cusp results from the fluctuations of many small excitations (low particle density-evaporated phase), whereas the tail to the left of the cusp is governed by a stretched exponential behaviour, reflecting the presence of a single large droplet (high particle density-condensed phase) with its interfacial energy playing here the dominant role.

§3. Theory

To give a mathematical basis to this physical picture, imagine that we have prepared the system at inverse temperature $\beta = 1/T > \beta_c$ in the positively magnetized phase with m slightly below the infinite-volume value $m_0(\beta) > 0$. The deviation (or excess)

$$\delta m \equiv m - m_0 = -2m_0 v_L/V \tag{3·1}$$

can be pictured as a (not necessarily connected) volume v_L containing the "wrong" phase of magnetisation $-m_0$ (i.e., of inverted spins with the majority being in the "$-$" state). This volume can be decomposed as $v_L = v_d + v_b$, where $v_d = \lambda v_L$ is the size of a large droplet and $v_b = (1-\lambda)v_L$ the integrated volume of many small bubbles. Correspondingly the (negative) magnetisation excess may be decomposed as $\delta m = \delta m_d + \delta m_b$. This decomposition into one large and many small droplets is nontrivial but makes sense, since by isoperimetric arguments it can be shown that no droplets of intermediate size can exist.[6] The parameter λ will now be determined by optimizing the free-energy contributions of these two types of excitations. The fluctuations of the small bubbles contribute a Gaussian factor,

$$\exp\left[-\beta V \frac{(\delta m_b)^2}{2\chi}\right] = \exp\left[-\beta V \frac{2m_0^2 (v_b/V)^2}{\chi}\right] , \tag{3·2}$$

where $\chi = \chi(\beta) = \beta V \left[\langle m^2\rangle - \langle m\rangle^2\right]$ is the susceptibility in the thermodynamic limit, whereas for the large droplet the interfacial free energy $\tau_W(\beta)$ per unit volume of an optimal Wulff shape[13)–15)] matters, leading in two dimensions to a contribution

$$\exp\left[-\beta\tau_W \sqrt{v_d}\,\right] . \tag{3·3}$$

Combining these two factors, we arrive at*)

$$\exp\left[-\beta \frac{2m_0^2(1-\lambda)^2 v_L^2}{\chi V} - \beta\tau_W\sqrt{\lambda v_L}\right] = \exp\left[-\beta\tau_W\sqrt{v_L}\,\Phi_\Delta(\lambda)\right] , \tag{3·4}$$

where

$$\Phi_\Delta(\lambda) = \sqrt{\lambda} + \Delta(1-\lambda)^2 \tag{3·5}$$

contains the dependence on the parameter λ interpolating between the bubble ($\lambda \to 0$) and droplet ($\lambda \to 1$) dominated phase. Which of the two possibilities wins, is governed by the parameter

$$\Delta = 2\frac{m_0^2}{\chi\tau_W}\frac{v_L^{3/2}}{V} , \tag{3·6}$$

which depends on the model specific (infinite-volume) quantities m_0, χ, and τ_W at the given temperature. To keep Δ fixed when increasing the system size V, one has to scale $\delta m \propto v_L/V \propto V^{-1/3}$.

At fixed Δ, the favored configuration follows by minimising $\Phi_\Delta(\lambda)$ with respect to λ. A glance at Fig. 2 shows a situation reminiscent of a first-order phase transition:

*) Note that the β-factor in Eqs. (3·2)–(3·4) was inadvertently omitted in Ref. 12).

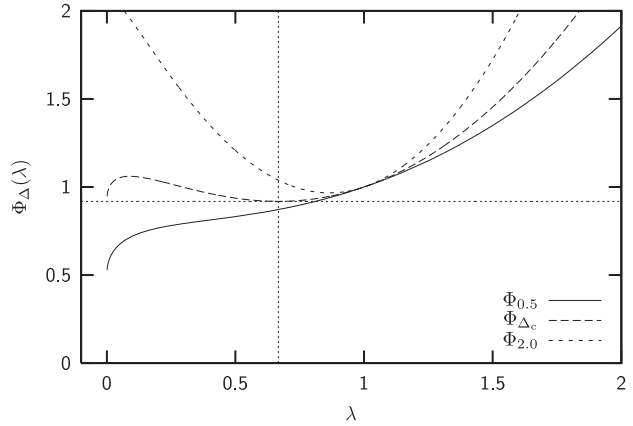

Fig. 2. The function $\Phi_\Delta(\lambda)$ for three characteristic values of the parameter Δ defined in Eq. (3·6). At $\Delta_c = (1/2)(3/2)^{3/2} \approx 0.9186$ the absolute minimum at $\lambda = 0$ for $\Delta < \Delta_c$ jumps to a non-trivial value $\lambda \geq 2/3$ (dashed vertical line) for $\Delta > \Delta_c$.

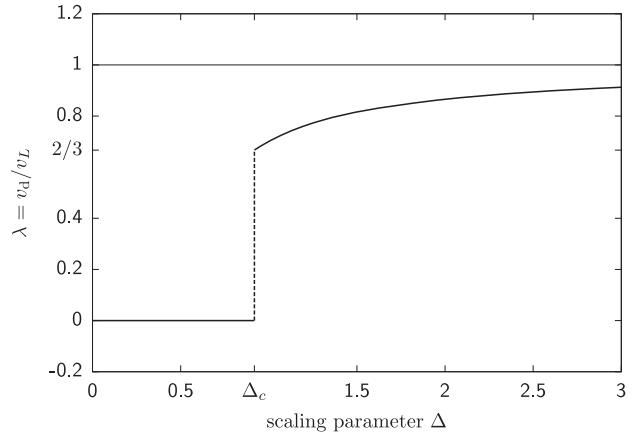

Fig. 3. Analytic solution $\lambda = \lambda(\Delta)$ obtained by minimization of Eq. (3·5).

for $\Delta < \Delta_c$ the global minimum is reached at $\lambda = 0$ (bubble dominated phase), whereas at the condensation point Δ_c the optimal value of λ jumps to a nontrivial solution $\lambda = \lambda(\Delta) > 0$ (droplet dominated phase) for $\Delta > \Delta_c$. One obtains $\Delta_c = (1/2)(3/2)^{3/2} \approx 0.9186$ and a jump to $\lambda_c = 2/3$, cf. Fig. 3 where the solution $\lambda = \lambda(\Delta)$ is plotted.

The free-energy barrier at $\Delta = \Delta_c$ (cf. Fig. 2) takes its maximum value $\Delta F = F_{\max} - F_{\min} = \tau_W \sqrt{v_L}\,(\Phi_{\Delta_c,\max} - \Phi_{\Delta_c,\min}) = \tau_W \sqrt{v_L}\, 3(2-\sqrt{3})/4\sqrt{2}$ at $\lambda_{\max} = (2-\sqrt{3})/3 \approx 0.089$. Using Eq. (3·6) to express v_L in terms of Δ_c, one obtains

$$\Delta F = \left(\frac{1}{2}\right)^{1/3} \frac{3(2\sqrt{3}-3)}{8} \tau_W \left(\frac{\chi \tau_W}{2m_0^2}\right)^{1/3} V^{1/3} \approx 0.1381 \tau_W \left(\frac{\chi \tau_W}{2m_0^2}\right)^{1/3} V^{1/3}. \quad (3·7)$$

Inserting the parameters for the square lattice Ising model with nearest-neighbour interactions at $T = 1/\beta = 1.5$ (see Table I below), one ends up with the explicit

result

$$\beta\Delta F \approx 0.1522\, L^{2/3}\,. \tag{3·8}$$

§4. Simulations

Since the theoretical predictions in the last section only apply to the infinite-size limit and, strictly speaking, only to the square lattice Ising model with nearest-neighbour (NN) interactions, two questions emerge naturally: (*i*) How fast do finite systems approach the limiting behaviour? And (*ii*) does the Ising model with an extended range of interaction or on different two-dimensional lattice types behave similarly? To answer these questions we have performed Monte Carlo computer simulations for increasing system sizes of (*i*) square lattices with NN interactions[12),16)] and (*ii*) next-nearest-neighbour (NNN) interactions as well as of triangular lattices with NN interactions.[16)] In addition, we also analyzed in case (*i*) the finite-size scaling behaviour of the associated free-energy barrier.

Our choice of the simulation temperature $T \approx (2/3)T_{\mathrm{c}}$ is a compromise between simulation speed (freezing of the spin-flip dynamics at too low temperatures) and compactness of the droplet (which becomes a fractal object at T_{c}). The main observable is the fraction of excess magnetisation in the largest droplet, $\lambda = v_{\mathrm{d}}/v_L$, as a function of v_L, which can be tuned via (3·1) by varying the magnetisation. Equation (3·6) then determines the scaling variable $\Delta = \Delta(v_L, m_0, \chi, \tau_{\mathrm{W}})$, provided the infinite-volume parameters m_0, χ, and τ_{W} are known.

4.1. *NN square lattice*

Let us first consider the NN square lattice, where the spontaneous magnetisation is given by the Onsager-Yang formula[17),18)] $m_0(\beta) = \left(1 - \sinh^{-4}(2\beta)\right)^{1/8}$ and $\tau_{\mathrm{W}}(\beta) = 2\sqrt{W}$ follows from the volume of the Wulff plot,[19)]

$$W = \frac{4}{\beta^2}\int_0^{\beta\sigma_0} dx \cosh^{-1}\left[\frac{\cosh^2(2\beta)}{\sinh(2\beta)} - \cosh(x)\right], \tag{4·1}$$

with $\sigma_0 = 2 + \ln[\tanh(\beta)]/\beta$ denoting the interface tension of an interface running along one of the two coordinate directions (e.g., (1,0) in standard crystallographic notation). The susceptibility is not known exactly, but an extremely long series expansion in $u = [2\sinh(2\beta)]^{-1}$, $\chi(\beta) = \beta\sum_{i=0}^{323} c_i u^{2i}$, gives very accurate results.[20)] The critical temperature $T_{\mathrm{c}} = 2/\ln(1+\sqrt{2})$ and all relevant parameters at the simulation temperature $T = 1.5 \approx 0.66\, T_{\mathrm{c}}$ are collected in Table I.

In a first step we checked the relevant region of the magnetisation. This was done

Table I. Infinite-volume magnetisation m_0, susceptibility χ and Wulff interface free energy per unit volume τ_{W}, entering the parameter $\Delta = \Delta(v_L, m_0, \chi, \tau_{\mathrm{W}})$ defined in Eq. (3·6).

model	T	T_{c}	T/T_{c}	m_0	χ	τ_{W}	$2m_0^2/\chi\tau_{\mathrm{W}}$
NN square	1.500	2.269	0.6610	0.9865	0.02708	4.245	16.93
NN triangular	2.400	3.641	0.6592	0.9829	0.01959	7.507	13.14
NNN square	3.500	5.258	0.6657	0.9741	0.01963	10.298	9.39

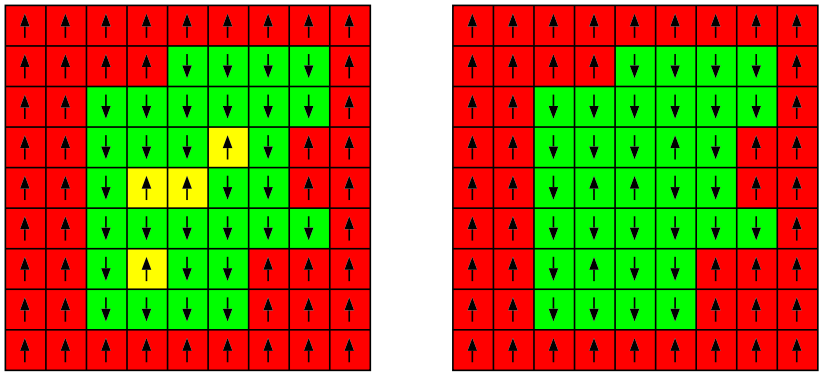

Fig. 4. Sketch of a large droplet containing overturned spins in its interior (left), which must be counted when measuring its volume v_{d}. This is achieved by a so-called "flood-fill" algorithm (right).

by performing multimagnetic simulations[21)–24)] and inspecting the distribution of the magnetisation as shown in Fig. 1 visually. For the larger system sizes the distribution exhibits a clear cusp around m_{c} which divides the evaporated and condensed region.

Next, we chose for each lattice size the same set of 38 values $\tilde{\Delta}_i = \{0.00, 0.10, ...\} \approx \Delta_i$, with an emphasis on the vicinity of Δ_{c}. The corresponding values of the total magnetisation M_i (obtained by first using (3·6) to calculate v_L and then (3·1)) must be rounded to the next allowed integer value and then the true $v_{L,i}$ and Δ_i are calculated backwards. The constraint of a constant magnetisation M_i ("micromagnetic ensemble") was enforced in the simulations by utilising a Metropolis update with Kawasaki dynamics exchanging pairs of unaligned spins. Every simulation ran 20 000 sweeps for the thermalisation and 200 000 sweeps for measurements, where one sweeps comprises V attempted spin exchanges. To obtain the statistical error bars reliably, 10 independent simulations were run for each data point. After every sweep a cluster decomposition was performed using the Hoshen-Kopelman[25)] algorithm and the volume v_{d} of the largest droplet was measured yielding for fixed v_L the desired fraction λ. It should be noted that, in the present context, the volume or size of the cluster *does* include overturned spins within the cluster (in contrast to percolation studies or improved estimators in cluster-update simulations[26)]), cf. Fig. 4. Our simulations are so sensitive that the proper counting of the cluster size turned out to be indeed crucial. Technically, this was handled by a so-called "flood-fill" routine[27)] that ran after the Hoshen-Kopelman algorithm. In essence, it starts from an inside spin and stops when a spin that belongs to the background is reached. Very rarely ambiguous cases can occur at the droplet boundary which can be detected automatically and were taken care of by inspection.

Our main result, the fraction $\lambda = \lambda(\Delta)$ for various lattice sizes, is shown in Fig. 5. The solid line represents the analytical curve obtained by the minimization of $\phi_\Delta(\lambda)$ in Eq. (3·5), which is the exact result in the infinite-volume limit. In the simulations we observe rather strong finite-size effects which smear out the transition, but for the larger lattice sizes the numerical data clearly approach the theoretical

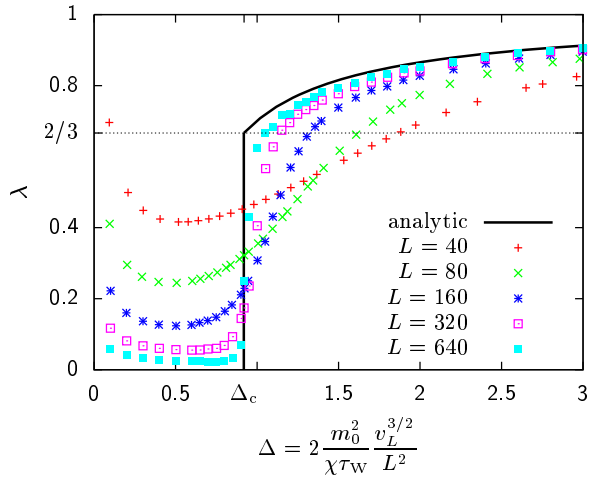

Fig. 5. Fraction of excess magnetisation $\lambda = v_{\mathrm{d}}/v_L$ in the largest droplet for NN square lattices of linear extent $L = 40, 80, \ldots, 640$ at the temperature $T = 1.5 \approx 0.66\,T_{\mathrm{c}}$. The error bars are much smaller than the size of the data symbols. The solid line shows the asymptotic analytic prediction for $L \to \infty$.

curve. The jump from $\lambda \approx 0$ to $\lambda \approx 2/3$ at $\Delta_{\mathrm{c}} \approx 0.9186$ confirms the theoretical prediction that at the evaporation/condensation transition 2/3 of the excess of the magnetisation goes into the large droplet while the rest remains in the background fluctuations. The apparent increase of λ for $\Delta \to 0$ can be explained by the fact that the minimal cluster size is 1 and not an arbitrarily small fraction. In contrast, the excess that can be fixed analytically using Eq. (3·6) can be much smaller than 1.

4.2. *NN triangular lattice*

Also for the NN triangular lattice all parameters are known exactly or at least to very high precision. Here the critical temperature is[28] $T_{\mathrm{c}} = 4/\ln 3$, the spontaneous magnetisation reads[29),*] $m_0(\beta) = \left\{1 - 16e^{-12\beta}/\left[\left(1+3e^{-4\beta}\right)\left(1-e^{-4\beta}\right)^3\right]\right\}^{1/8}$, and for the susceptibility a sufficiently long series expansion in $u = \exp(-4\beta)$ is available,[30] $\chi(\beta) = \beta\sum_{i=1}^{21} c_i u^i$. The interfacial free energy $\tau_W = 2\sqrt{W}$ is more complicated than for the square lattice, but still known exactly in the form $W(\beta) = 6\int_0^{\pi/6} d\theta\, r^2(\theta)$, with $r(\theta)$ given as the solution of a β-dependent implicit equation.[31] The numerical values of these quantities at the simulation temperature $T = 2.4 \approx 0.66\,T_{\mathrm{c}}$ are again compiled in Table I.

Due to the geometry of the triangular lattice with its hexagonal unit cells some care is necessary with the proper normalization.[16] When all quantities are normalized to the total number of spins, the Δ parameter requires a geometric correction factor $\alpha = \sqrt{2/\sqrt{3}} \approx 1.075$, which is just the inverse square root of the hexagonal

*) Note an obvious printing error in Eq. (30) of Ref. 16).

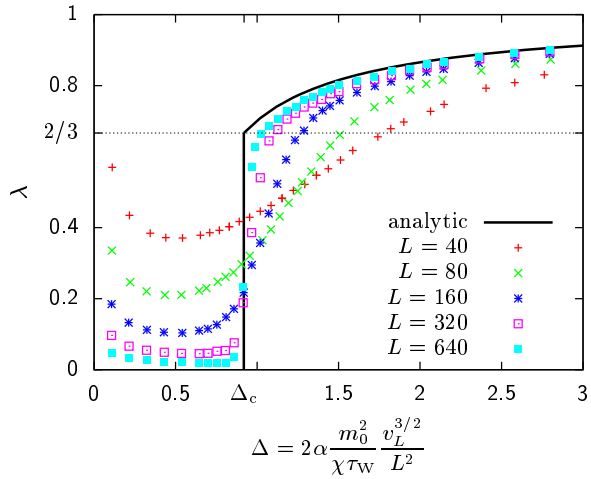

Fig. 6. Fraction of excess magnetisation $\lambda = v_{\rm d}/v_L$ in the largest droplet for NN triangular lattices of linear extent $L = 40, 80, \ldots, 640$ at the temperature $T = 2.4 \approx 0.66\,T_{\rm c}$. The error bars are much smaller than the size of the data symbols. The solid line shows the asymptotic analytic prediction for $L \to \infty$.

unit cell volume $\sqrt{3}/2$ for links of unit length. Hence, here we have to plot λ against

$$\Delta = 2\alpha \frac{m_0}{\chi \tau_W} \frac{v_L^{3/2}}{L^2}\,. \tag{4·2}$$

By employing the same simulation methodology as for the square lattice, we obtain the result shown in Fig. 6, which very much resembles the NN square lattice case in Fig. 5.

4.3. *NNN square lattice*

Whereas for both lattice types with NN interactions analytical values for the parameters in Table I are available, for the NNN square lattice one first has to compute numerical estimates. The critical temperature is known to sufficient accuracy from independent transfer-matrix studies[32] and recent Monte Carlo simulations combined with finite-size scaling analyses,[33] which consistently give $T_{\rm c} = 5.25783$. The magnetisation and susceptibility are rather easily obtained in separate Monte Carlo simulations, since at $T \approx (2/3)T_{\rm c}$ the spatial correlation length is very small and already for moderate lattice sizes rather precise estimates can be obtained.

Much more demanding is the estimate of the Wulff free energy. Among the various methods described in Ref. 16) we picked for the present analysis the following one: for NNN Ising droplets, the low-temperature Wulff shape is an octagon, i.e., it is quite close to the high-temperature (low-interface-tension) circular shape. It is therefore a reasonable approximation to assume an angle independent interface tension σ_0, which can be estimated for a planar interface by finite-size scaling[33] and translated into $\tau_W \approx 2\sqrt{\pi}\sigma_0$. Performing this procedure at $T = 3.5 \approx 0.66\,T_{\rm c}$, we obtained $\tau_W \approx 2\sqrt{\pi} \times 2.905 = 10.298$. The numerical values of all required quantities are compiled in Table I. Compared to our previous study[16] at the higher temper-

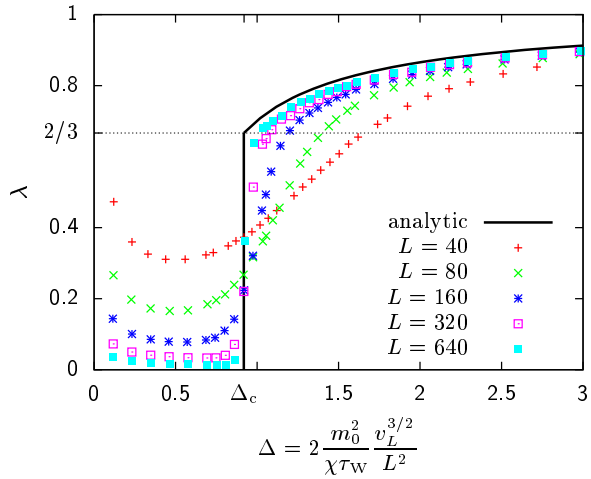

Fig. 7. Fraction of excess magnetisation $\lambda = v_{\mathrm{d}}/v_L$ in the largest droplet for NNN square lattices of linear extent $L = 40, 80, \ldots, 640$ at the temperature $T = 3.5 \approx 0.66\,T_{\mathrm{c}}$. The error bars are much smaller than the size of the data symbols. The solid line shows the asymptotic analytic prediction for $L \to \infty$.

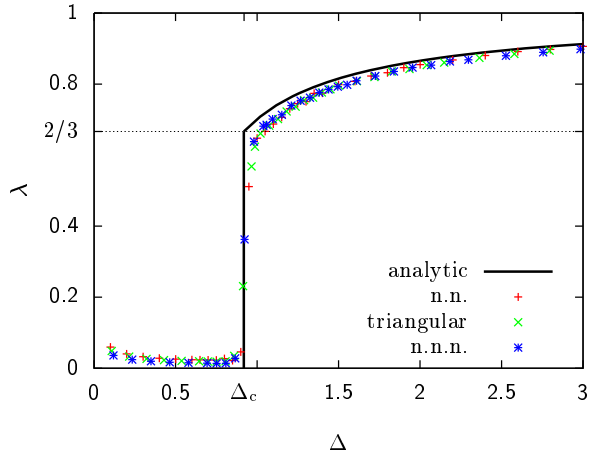

Fig. 8. Comparison of the fraction λ for the largest size $L = 640$ of the three considered Ising models: NN square, NN triangular, and NNN square lattice. In all three cases the simulation temperature is chosen as $T \approx 0.66\,T_{\mathrm{c}}$.

ature $T = 4.0$, the differences are quite sizeable. Since the previously considered temperature corresponds to $T \approx 0.76\,T_{\mathrm{c}}$, we decided here to repeat the whole set of simulations for $T \approx 0.66\,T_{\mathrm{c}}$, that is for $T = 3.5$, in order to allow a direct comparison with the results for the NN square and triangular lattice.

The fraction of excess magnetisation $\lambda = v_{\mathrm{d}}/v_L$ in the largest droplet versus Δ is plotted in Fig. 7. We see that also for the extended range of interactions the overall finite-size scaling behaviour looks very much the same as for the NN square and triangular lattices.

A quantitative comparison is shown in Fig. 8 for our largest lattice size $L =$

640. When the relative temperature T/T_c has the same value for the three lattice/interaction types, then the $\lambda(\Delta)$ curves can be hardly distinguished. Microscopic details thus do not seem to matter much in this representation even though T_c of the three models and the parameters entering Δ differ quite considerably, cf. Table I. The approach of the infinite-volume limit does of course depend on the chosen temperature. For this reason a similar comparison in Ref. 16) with the NNN square model simulated at $T = 4$ looked far less "universal".

4.4. *Free-energy barrier*

Having established the insensitivity of the droplet condensation mechanism to microscopic details such as the lattice structure or the range of interactions, we now turn to an exploratory analysis of the coexistence region around Δ_c for the simplest case of a NN square lattice. Snapshots of actual configurations in the two phases are shown for a small system in Fig. 9. The probability distributions of $\lambda = v_d/v_L$ obtained in micromagnetic simulations with a fixed value of m (respectively Δ) close to m_c (respectively Δ_c) plotted in Fig. 10 exhibit for the larger lattice sizes a clear two-phase signal: the system is either in the evaporated bubble phase where $\lambda \approx 0$ or in the condensed phase where $\lambda \approx 2/3$, marked by the vertical line. More precisely, the magnetisation m (or equivalently Δ) was adjusted for each lattice size such that the two peaks are roughly of equal height.

The minimum between the two peaks corresponds to the free-energy barrier (3·7), (3·8) depicted in Fig. 2, i.e., the ratio of the minimum to the maximum should decrease with system size L as $\exp(-\beta\Delta F) = \exp(-cL^{2/3})$ with $c = 0.1522$ at $T = 1.5$. This scaling behaviour is tested in Fig. 11. Allowing a power-like prefactor $\propto L^{\kappa}$, a fit through the data points for $L \geq 90$ yields $c = 0.211 \pm 0.003$ with a goodness-of-fit parameter $Q = 0.22$. Even though this estimate is quite far off the expectation, if we fix $c_1 = 0.1522$ and use the fit range $L \geq 170$, we obtain a perfectly compatible fit with a goodness of $Q = 0.16$. As can be seen in Fig. 11, for the larger lattice sizes the two fits are hardly distinguishable which makes it so difficult to estimate the parameter c reliably.

This barrier plays an important role for the understanding of the dynamics

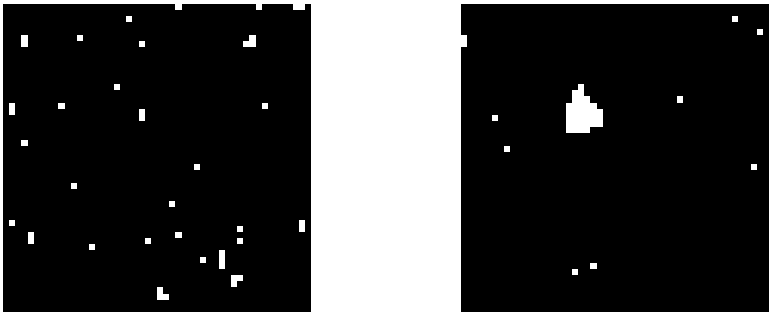

Fig. 9. Two snapshots of a $L = 50$ NN square lattice for $T = 1.5$ at the evaporation/condensation magnetisation m_c. Left: Evaporated system with a large number of very small bubbles (1 to 3 spins). Right: Condensed system with a single large droplet that has absorbed most of the small bubbles.

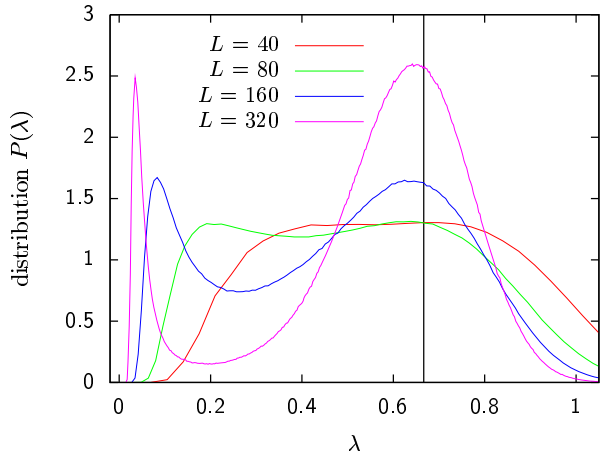

Fig. 10. Probability distribution of the fraction $\lambda = v_{\mathrm{d}}/v_L$ close to the evaporation/condensation transition on NN square lattices at $T = 1.5$, exhibiting a clear two-phase signal. The magnetisation m resp. Δ parameter is adjusted such that the two peaks are of equal height. The minimum between the peaks corresponds to the free-energy barrier in Fig. 2.

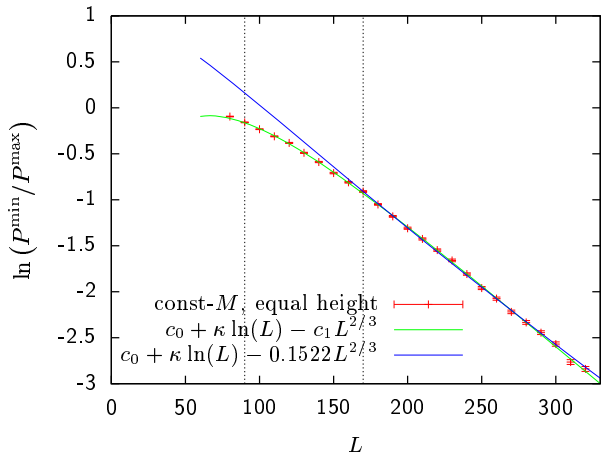

Fig. 11. Ratio of the peak minimum to the maximum in Fig. 10 versus lattice size. The vertical lines mark the lower bounds of the fit ranges for which the goodness-of-fit parameter $Q > 0.1$.

of simulations in the multicanonical ensemble or, in this context, more precisely multimagnetical simulations.[21] The main ingredient of this method are iteratively determined auxiliary weight factors $W(m)$ which, when multiplied with the usual canonical Boltzmann factor, can be adjusted to produce a flat distribution of the magnetisation. In such a situation one would naively expect a random walk behaviour of the Monte Carlo dynamics and hence only a power-law scaling of the autocorrelation time τ with the lattice size L.[22] The free-energy barrier at the evaporation/condensation point teaches us, however, that this cannot be true since the system cannot easily pass through the point m_{c}. Rather, it first has to overcome the free-energy barrier (3·8) in a direction "orthogonal" to the magnetisation. The

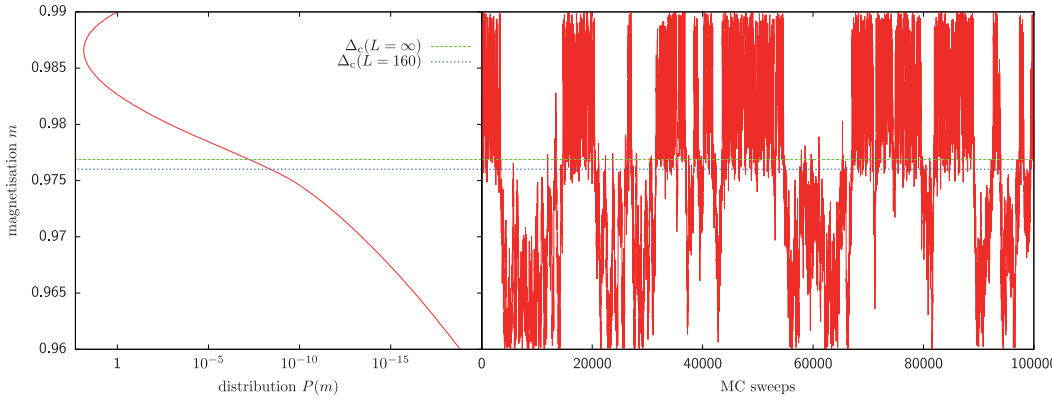

Fig. 12. Time evolution of a multimagnetical Ising model simulation on a 160×160 NN square lattice at $T = 1.5$ close to the evaporation/condensation point m_c, where the cusp is not yet very pronounced. One clearly sees, however, that the system's path through the state space is usually reflected at $m \approx m_c$ and only every few thousand sweeps the barrier (3·8) is overcome.

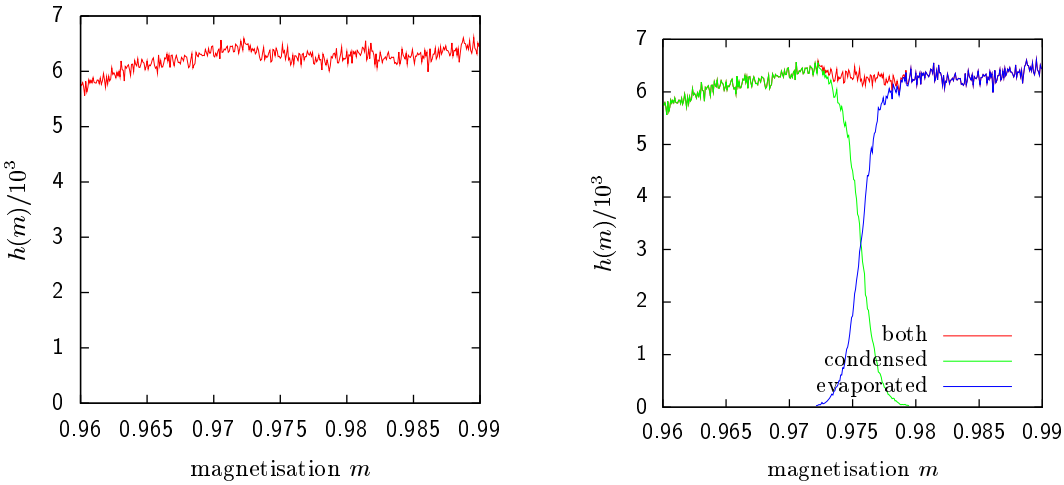

Fig. 13. Left: Flat multimagnetical histogram resulting from the time evolution shown in Fig. 12. Right: Decomposition of the histogram into the contributions from the condensed (small m) and evaporated (large m) phase.

time series of a multimagnetical simulation around m_c in Fig. 12 shows that this barrier indeed has a significant impact. Note that despite this barrier the resulting multimagnetical histogram is perfectly flat. This is demonstrated in Fig. 13, where it is also shown how the contributions from the condensed and evaporated phase add up to produce the total histogram.

In micromagnetic simulations with fixed magnetisation $m = m_c$, the measured (integrated) autocorrelation time τ_{int} should reflect this barrier asymptotically in the scaling behaviour $\tau_{\text{int}} \simeq \exp(\beta \Delta F) = \exp(cL^{2/3})$. Our results of long simulations with 10 million sweeps at m_c for many lattice sizes up to $L = 330$ are shown in Fig. 14. Using the data for $L \geq 140$, the ansatz $\ln(\tau_{\text{int}}) = c_0 + \kappa \ln(L) + c_1 L^{2/3}$

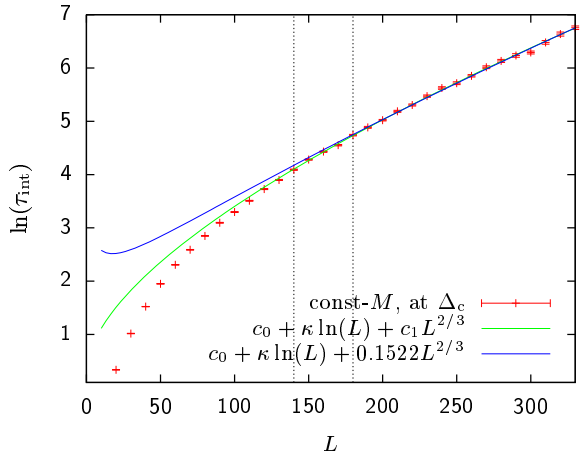

Fig. 14. (Integrated) autocorrelation times of micromagnetic simulations at constant $m = m_c$ versus lattice size. The vertical lines mark the lower bounds of the fit ranges for which the goodness-of-fit parameter $Q > 0.1$.

yields $c_1 = 0.124 \pm 0.008$ with goodness-of-fit parameter $Q = 0.18$. This estimate is somewhat closer to the theoretically expected value $c = 0.1522$, but also here it clearly deviates by $3 - 4$ error bars. Similarly to the situation for $P^{\min}/P^{\max}$, by constraining the fit parameter $c_1 = c$ to its theoretical value and fitting only c_0 and κ, we obtain for $L \geq 180$ again a perfectly acceptable fit with goodness-of-fit $Q = 0.28$. Also here the two fits plotted in Fig. 14 are practically indistinguishable for larger lattice sizes. We are currently trying to improve the numerical determination of the parameter c_1 by extending the simulations to bigger systems, but this is quite a time-consuming task.

Finally it should be noted that the magnitude of the autocorrelation time in Fig. 14 is much smaller than the estimate one can read off from the time evolution of the *multi*magnetical simulation on the 160×160 lattice shown in Fig. 12. This is because in multimagnetical simulations the system spends a lot of time away from m_c, either in the evaporated or condensed phase. The asymptotic scaling behaviour with system size, however, should also be governed by the same exponential law as for the constrained simulations with fixed magnetisation.

§5. Concluding remarks

The results of our Monte Carlo simulations of the droplet condensation process in the two-dimensional Ising lattice-gas model clearly confirm the mathematical predictions of Biskup et al.[6] and extend their exact analysis for asymptotically large systems to practically accessible system sizes. The observed finite-size scaling behaviour matches with increasing system size perfectly with the predicted infinite-volume limit. By comparing square and triangular lattices with next-neighbour interactions and a square lattice with next-nearest-neighbour interactions, we obtain compelling evidence for the insensitivity of the droplet condensation mechanism on

microscopic details provided the reduced temperature T/T_c is kept fixed. Strictly speaking, for technical reasons, the mathematical treatment of Biskup et al.[6] is restricted to square lattices with nearest-neighbour couplings only. Our results thus show that the arguments in Ref. 6) can indeed be carried over to other lattice types and interactions as well, as expected on physical grounds. All simulations were performed in thermal equilibrium and the suppression of droplets of intermediate size could be unambiguously verified.

The observed double-peak structure of the distribution of the fraction λ of particles in the largest droplet at the evaporation/condensation transition implies a free-energy barrier, similar to a first-order phase transition. Extrapolations of our results for finite systems to the infinite-volume limit are in qualitative agreement with the theoretical expectation. By analyzing the ratio of the peak minimum to the maximum in simulations with fixed magnetisation (adjusted such that the two peaks are of equal height), we clearly observe with increasing lattice size L an exponential scaling compatible with $\exp(-c\,L^{2/3})$. A precise numerical determination of the parameter c, however, turns out to be difficult for the available lattice sizes. Alternatively, by measuring (integrated) autocorrelation times τ_{int} in simulations with the magnetisation fixed directly at the evaporation/condensation point Δ_c, we also find a compatible asymptotic scaling behaviour $\tau_{\mathrm{int}} \simeq \exp(c\,L^{2/3})$, but the parameter c is again difficult to estimate reliably with the present data set. Presumably much larger lattices are needed to arrive at a firm estimate. In multimagnetical simulations with a flat magnetisation distribution, this free-energy barrier is not directly visible when monitoring the magnetisation alone. Rather, it appears as a "hidden" obstacle in an "orthogonal" direction of phase space, which is, however, clearly reflected by a slowing down of the performance of the simulations.

Currently we are performing similar simulations and analyses for the three-dimensional case, where a similar behaviour is expected in the thermodynamic limit. It appears, however, numerically much harder to reach the scaling region. Once the relevant length scales are fully understood, off-lattice simulation studies with Lennard-Jones particles in a similar vein would be a very interesting project with many applications of practical relevance.

Acknowledgements

This work was initiated and partially supported by the Yukawa International Program for Quark-Hadron Sciences (YIPQS). WJ wishes to thank Hisao Hayakawa and Nobuyasu Ito for their kind hospitality during his stay in Kyoto. We also gratefully acknowledge support by the Deutsche Forschungsgemeinschaft (DFG) under grant Nos. JA483/22-1 & 23-1, the EC RTN-Network "ENRAGE": *Random Geometry and Random Matrices: From Quantum Gravity to Econophysics* under grant No. MRTN-CT-2004-005616, the DFG Research Group FOR877, and the DFH-UFA German-French Graduate College *Statistical Physics of Complex Systems* under grant No. CDFA-02-07.

References

1) M. E. Fisher, Rep. Prog. Phys. **30** (1967), 615.
2) K. Binder and M. H. Kalos, J. Stat. Phys. **22** (1980), 363.
3) H. Furukawa and K. Binder, Phys. Rev. A **26** (1982), 556.
4) J. Lee, M. A. Novotny and P. A. Rikvold, Phys. Rev. E **52** (1995), 356.
   M. Pleimling and W. Selke, J. of Phys. A **33** (2000), L199.
   M. Pleimling and A. Hüller, J. Stat. Phys. **104** (2001), 971.
5) T. Neuhaus and J. S. Hager, J. Stat. Phys. **113** (2003), 47.
6) M. Biskup, L. Chayes and R. Kotecký, Europhys. Lett. **60** (2002), 21; Commun. Math. Phys. **242** (2003), 137.
7) M. Biskup, L. Chayes and R. Kotecký, J. Stat. Phys. **116** (2003), 175.
8) K. Binder, Physica A **319** (2003), 99.
9) P. Virnau, L. G. MacDowell, M. Müller and K. Binder, in *Computer Simulation Studies in Condensed Matter Physics XVI*, Springer Proceedings in Physics, Vol. 95, ed. D. P. Landau, S. P. Lewis and H.-B. Schüttler (Springer, Berlin, 2004), p. 129.
   L. G. MacDowell, P. Virnau, M. Müller and K. Binder, J. Chem. Phys. **120** (2004), 5293.
   K. Binder, M. Müller, P. Virnau and L. G. MacDowell, Adv. Polymer Science **173** (2005), 1.
10) L. G. MacDowell, V. K. Shen and J. R. Errington, J. Chem. Phys. **125** (2006), 034705.
11) A. Nußbaumer, E. Bittner and W. Janke, PoS(LAT2005)252.
12) A. Nußbaumer, E. Bittner, T. Neuhaus and W. Janke, Europhys. Lett. **75** (2006), 716.
13) G. Wulff, Z. Kristallogr. Mineral. **34** (1901), 449.
14) S. B. Shlosman, Commun. Math. Phys. **125** (1989), 81.
15) R. L. Dobrushin, R. Kotecký and S. B. Shlosman, *Wulff Construction. A Global Shape from Local Interaction* (Amer. Math. Soc., Providence, RI, 1992); J. Stat. Phys. **72** (1993), 1.
16) A. Nußbaumer, E. Bittner and W. Janke, Phys. Rev. E **77** (2008), 041109.
17) L. Onsager, Nuovo Cim. Suppl. **6** (1949), 261.
18) C. N. Yang, Phys. Rev. **85** (1952), 808.
19) K. Leung and R. K. P. Zia, J. of Phys. A **23** (1990), 4593.
20) W. P. Orrick, B. G. Nickel, A. J. Guttmann and J. H. H. Perk, Phys. Rev. Lett. **86** (2001), 4120; J. Stat. Phys. **102** (2001), 795.
21) B. A. Berg and T. Neuhaus, Phys. Rev. Lett. **68** (1992), 9.
   B. A. Berg, U. Hansmann and T. Neuhaus, Phys. Rev. B **47** (1993), 497; Z. Phys. B **90** (1993), 229.
22) W. Janke, in *Computer Simulations of Surfaces and Interfaces*, NATO Science Series II, Mathematics, Physics and Chemistry, Vol. 114, ed. B. Dünweg, D. P. Landau and A. I. Milchev (Kluwer, Dordrecht, 2003), p. 137.
23) B. A. Berg, Fields Inst. Commun. **26** (2000), 1.
24) W. Janke, Physica A **254** (1998), 164; Lect. Notes Phys. **739** (2008), 79.
25) J. Hoshen and R. Kopelman, Phys. Rev. B **14** (1976), 3438.
26) W. Janke, in *Ageing and the Glass Transition*, ed. M. Henkel, M. Pleimling and R. Sanctuary, Lect. Notes Phys. **716** (Springer, Berlin, 2007), p. 207.
27) M. K. Agoston, *Computer Graphics and Geometric Modelling* (Springer, London, 2004).
28) R. J. Baxter, *Exactly Solved Models in Statistical Mechanics* (Academic Press, New York, 1982).
29) R. B. Potts, Phys. Rev. **88** (1952), 352.
30) M. F. Sykes, M. G. Watts and D. S. Gaunt, J. of Phys. A **8** (1975), 1448.
31) V. A. Shneidman and R. K. P. Zia, Phys. Rev. B **63** (2001), 085410.
32) M. P. Nightingale and H. W. J. Blöte, J. of Phys. A **15** (1982), L33.
33) A. Nußbaumer, E. Bittner and W. Janke, Europhys. Lett. **78** (2007), 16004.